RSC Chemical Biology

Accepted Manuscript

This article can be cited before page numbers have been issued, to do this please use: O. Gould, A. Gibney, R. Lynn, S. Poole, B. McGorman and A. Kellett, *RSC Chem. Biol.*, 2026, DOI: 10.1039/D6CB00097E.

ROYAL SOCIETY OF CHEMISTRY

rsc.li/rsc-chembio

View Article Online
DOI: 10.1039/D6CB00097E

ARTICLE

Rational Design of an Acridine-derived Click Chemistry-based Artificial Metallo-Nuclease

Received 00th January 20xx,
Accepted 00th January 20xx

DOI: 10.1039/x0xx00000x

Oliver Gould,† Alex Gibney,† Rebecca Lynn, Simon Poole, Bríonna McGorman,* and Andrew Kellett*

Artificial metallo-nucleases (AMNs) are metal complexes capable of cleaving nucleic acids and represent a promising therapeutic class. We recently established that copper(I)-catalysed azide-alkyne cycloaddition (CuAAC) click chemistry offers a versatile approach for building new minor groove targeting AMNs, epitomised by the Tri-Click (TC) series; here, three bidentate chelation sites comprising the N-triazole donor from the CuAAC reaction, together with the 'clicked' donor group, provide new ligand architectures that coordinate up to three bioactive copper(II) metal ions. Although the TC series are promising scaffolds, no route has yet been established to direct, or enhance their DNA recognition properties. Herein, we report a new method for hybridising click chemistry-based AMNs with acridine, a potent DNA intercalating agent. Motivation for generating this conjugate stems from the opportunity to combine multimodal DNA binding properties, namely, DNA intercalation via the acridine unit, and minor groove recognition and cleavage by the nuclease component. Two sites of the original TC scaffold were retained for copper chelation and DNA cleavage, thereby producing a Di-Click-Pyridine (DC-Py) unit, while the third site was repurposed for conjugation to the acridine (A) group. The resultant hybrid (DC-PyA) was then coordinated with copper(II) ions (Cu_2-DC-PyA) and the downstream direct and indirect DNA recognition properties and cleavage properties were examined, and activity resembling threading DNA intercalation was observed.

Introduction

There has been a sustained interest in the development of new artificial metallo-nucleases (AMNs),[1–6] in-part owing to the clinical success of bleomycin—an antineoplastic antibiotic that chelates Fe(II), binds to DNA, and promotes oxidative DNA damage through DNA-localised Fenton-type chemistry.[7–9] Recently, we reported a new strategy for AMN development using click chemistry, whereby the 1,2,3-triazole group formed during the copper(I)-catalysed azide-alkyne cycloaddition (CuAAC) reaction, together with proximal secondary alkynyl donors, chelates with up to three Cu(II) ions to form trinuclear 'Tri-Click' (TC) complexes.[10–12] Our most recent contribution in this area identified TC-Py (where Py = pyridine) as the most active AMN from a focused series of alkynyl donors with potential copper(II) ion chelating properties.[12] Mechanistic experiments involving molecular dynamics identified that two of the three triazole–Py arms in the Cu_3-TC-Py complex actively participate in DNA binding (**Figure 1a**), while the third arm does not directly contact the DNA surface. Although the third site likely enhances binding opportunities through it's dynamic motion, its remote positioning suggests a rational choice for incorporating a directing group. While gene-targeting vectors like triplex-forming oligonucleotides offer significant opportunities for sequence-specific targeting,[13–15] recent reviews highlight that conjugation of AMNs to established DNA-binding small molecules provides a direct method for AMN activity enhancement.[1,16] Acridine and its analogues have been used to this end by successfully enhancing the nuclease activity of various AMNs (**Figure 1b**),[17–21] and have further promoted nuclear localisation of Au(I) and ^{99m}Tc(I) complexes.[22,23] Here, we report Cu_2-DC-PyA (**Figure 1c**), a TC-inspired, click-assembled hybrid in which two Py-supported Cu(II) centres are retained for minor-groove cleavage while the third position is repurposed as an acridine intercalator, enabling cooperative copper-mediated nuclease activity and dual-mode DNA recognition.

Results and discussion

Synthesis

DC-PyA was prepared using multi-step synthesis outlined in **Figure 1d**. In order to generate a C_2-symmetric analogue of the recently reported TC-Py, we started by alkylating mesitol to generate **1**, prior to the installation of two azide handles in **2** by nucleophilic substitution with sodium azide.

School of Chemical Sciences, Dublin City University, Glasnevin, Dublin 9, Dublin, Ireland.
† Authors who contributed equally.
* andrew.kellett@dcu.ie

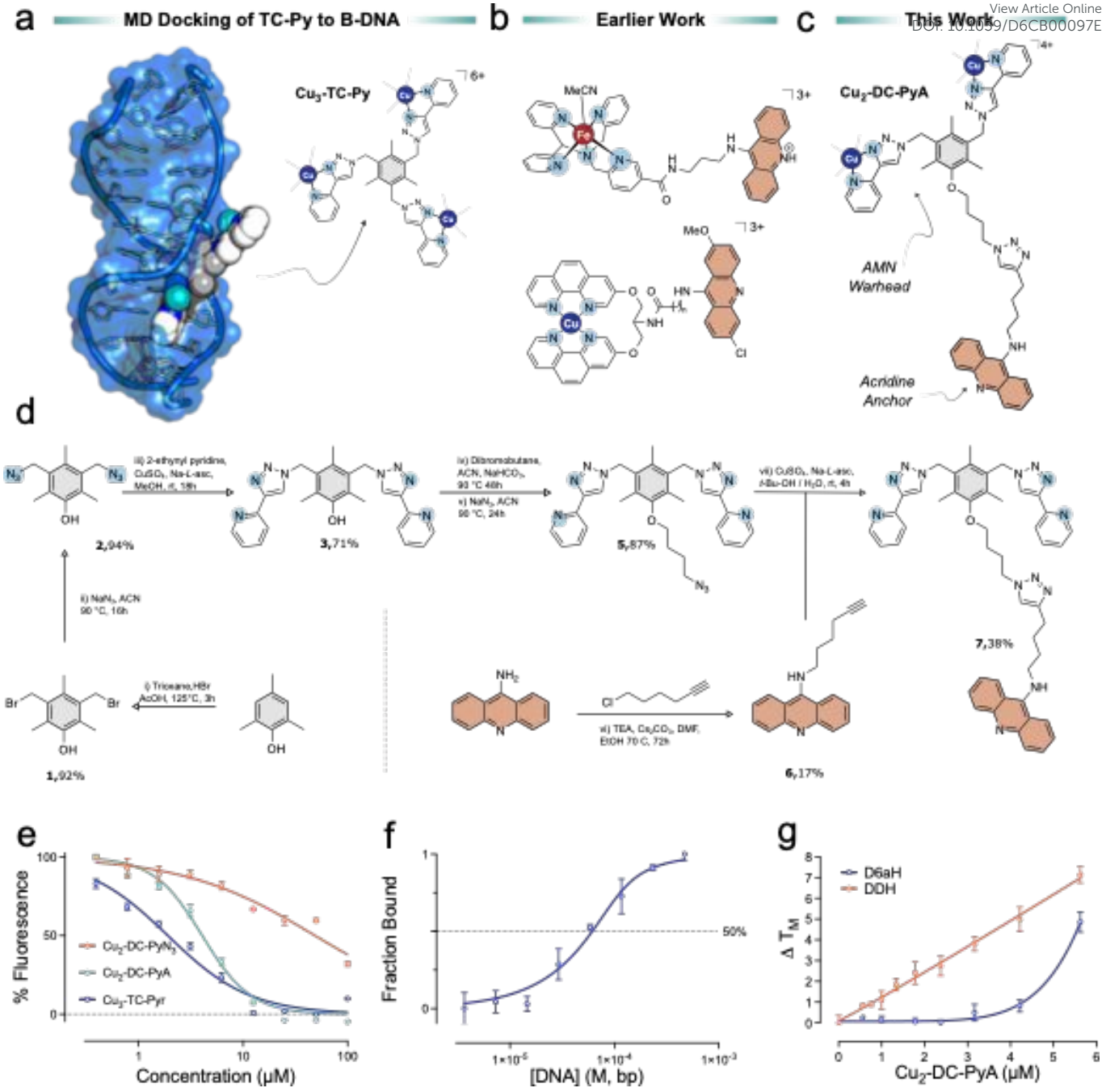

Figure 1: a) Previously reported Cu_3-TC-Py binds duplex DNA with an exposed "arm". **b**) Examples of AMNs that have shown enhanced activity upon conjugation to acridines. **c**) Structure prepared in this study, Cu_2-DC-PyA, a derivative of Cu_3-TC-Py where one arm has been replaced with an acridine anchor. **d**) Synthetic procedure for the synthesis of DC-PyA. **e**) Fluorescent intercalator displacement assays enabled calculation of apparent binding constants. Cu_2-DC-PyA shows enhanced binding affinity relative to its synthetic precursor Cu_2-DC-PyN_3 and similar affinity to the parent, Cu_3-TC-Py. **f**) Direct binding monitored by fluorescence upon titration of ctDNA, which enabled calculation of the direct binding constant of Cu_2-DC-PyA using the Bard model. **g**) Thermal melting analysis using FRET-modified DNA hairpins showed clear sequence discrimination. Non-linear regression included for presentation purposes only (concentration 10 μM and 7.5 μM were excluded due to condensation). All experiments were conducted in triplicate; all error bars indicate standard error of three values.

Subsequent CuAAC with 2-ethynyl pyridine then produced **3**, and the phenolic group allowed the incorporation of an alkynyl linker in **4** via Williamson ether synthesis using excess dibromobutane. Azidation of the resulting alkyl halide was next performed with sodium azide to generate DC-PyN_3 (**5**). In parallel, 9-amino acridine was alkylated via nucleophilic substitution to produce 9-hexynyl acridine (**6**). DC-PyN_3 and 9-hexynyl acridine were then combined in a second CuAAC reaction to provide the final ligand, DC-PyA (**7**). The seven-step, synthetic workflow provided a final product yield of 20% from the mesitylene starting material, predominantly diminished by the final CuAAC step with of **5** and **6,** which required chromatographic purification. The attempted synthesis of **6** under standard

View Article Online
DOI: 10.1039/D6CB00037F

nucleophilic substitution conditions, did not proceed (data not shown) and the reaction required use of caesium carbonate to promote formation of the desired intermediate, which showed poor chromatographic separation under flash conditions.[24] All synthetic targets were characterised by ^{1}H and ^{13}C NMR. Azides **2** and **5** were additionally characterised by Fourier Transform Infrared (FT-IR) spectroscopy and liquid chromatography-mass spectrometry (LC-MS) was carried out on the final product **(Figures S1-S12)**.

DNA binding studies

Apparent binding constants. Metal complex stocks were prepared *in-situ* by mixing DC-PyA and two molar equivalents of copper(II) nitrate trihydrate to produce Cu_2-DC-PyA. The DNA binding affinity of Cu_2-DC-PyA was initially evaluated using an ethidium bromide (EtBr)-based fluorescent intercalator displacement (FID) assay. Titration of a test compound into solutions of EtBr-saturated DNA results in competition and concentration-dependent depletion of EtBr fluorescence. Data from this assay can then be used to calculate an apparent DNA binding constant (K_{app}) using equation 1, where K_b is the equilibrium binding constant of EtBr, [EtBr] is the concentration of EtBr in the sample and C_{50} is the concentration of titrant required to reduce fluorescence by 50%.[25]

$$\textbf{Equation 1)}\ K_{app} = \frac{K_b[EtBr]}{C_{50}}$$

It is worth noting that FID assays are limited by their indirect nature and are affected by the K_b value used in equation 1 along other factors such as temperature, sequence composition, and buffer. It is also important that the same K_b value and experimental conditions are used between experiments if K_{app} values are to be compared. Accordingly, we used a K_b value of 8.8 x 10^6 M^{-1} and experimental conditions as recently reported[12] to allow comparison to Cu_3-TC-Py. Here, Cu_2-DC-PyA returned a K_{app} value of 2.71 x 10^7 M^{-1}, similar to the value of 5.8 x 10^7 M^{-1} previously reported for Cu_3-TC-Py and exceeding that of other TC complexes.[10–12] Interestingly, we found the K_{app} value of the target Cu_2-DC-PyA was an order of magnitude higher than the azide precursor Cu_2-DC-PyN_3 (K_{app} = 2.2 x 10^6 M^{-1}), which lacks the conjugated acridine unit.

Direct DNA binding analysis. FID assays are useful tools for the analysis of compounds with otherwise unsuitable spectroscopic properties, such as those lacking a chromophore or presenting a dominant spectral overlap with DNA.[26] However, the incorporation of acridine into Cu_2-DC-PyA allowed us to directly monitor DNA binding of this unit by fluorescence spectroscopy (**Figure S13**). Here, ctDNA was titrated into a buffered solution of Cu_2-DC-PyA (10 μM; 80 mM HEPES, 25 mM NaCl, pH 7.4), and fluorescence changes were monitored at λ_{ex} = 415 nm and λ_{em} = 455 nm (**Figure S14**). Results showed a clear increase in fluorescence with increasing DNA concentrations (**Figures S15** and **S16**). Data was modelled using the Bard equation (**Equations S1** and **S2**)[27,28] which best fit the data with a binding affinity of 6.5 x 10^5 M^{-1} and a stoichiometry of 5 bp per Cu_2-TC-PyA. Interestingly, this binding stoichiometry is lower than might be expected for a bifunctional molecule such as Cu_2-DC-PyA and may indicate a cooperative binding mode. The lower direct binding constant relative to K_{app} likely reflects the fact that only the acridine component contributes to the fluorescence signal in direct measurements. Since the dicopper unit lacks a chromophore and is therefore spectroscopically silent under these conditions, binding events mediated solely by the Cu_2-DC-Py component, through minor groove recognition in the absence of acridine intercalation are therefore not captured.

Thermal melting studies. Next, we evaluated the impact of Cu_2-DC-PyA binding on the thermodynamic stability of hairpin DNA targets using a FRET melting method **(Figures 1g** and **S17-19)**.[2] Here, hairpin DNA constructs were modified to contain FRET partners of 3′-Iowa Black® and 5′-Alexa Fluor™ 647. When annealed the proximity of the FRET pair results in fluorescence quenching, and when denatured, the FRET pair separate to give a fluorescence signal.[29]

The thermal denaturation of the hairpin can therefore be monitored through the fluorescence signal and the midpoint of the melting curve identified as the melting temperature (T_m).[30–32] To investigate the sequence selectivity of Cu_2-DC-PyA we monitored thermal melting changes (ΔT_m) using two hairpin sequences containing varying GC content: DDH, which contains 66% GC content and D6ah, which contains 33% GC content.

Here, we found that Cu_2-DC-PyA showed clear linear stabilisation of the DDH hairpin with an ΔT_m of ~5 °C upon exposure to 5 μM of the complex. In contrast, the D6aH hairpin was minimally stabilised with a maximum ΔT_m of < 1.5 °C at the highest complex exposure. These results indicate that incorporation of the acridine moiety into Cu_2-DC-PyA enhances the GC-sequence selectivity, likely reflecting an additive effect of GC-selectivity by 9-aminoacridine derivatives.[33] This enhanced GC selectivity supports the intended intercalative role of the acridine unit suggesting the acridine motif engages DNA as designed.

Viscosity studies. A key feature of intercalation is the extension of the DNA double helix as the intercalator participates in π-stacking interactions with successive nucleobases.[34] Consequently, methods sensitive to measuring hydrodynamic changes can be used to characterise DNA intercalation with viscosity being one of the most readily accessible methods.[35] To validate intercalation by the acridine moiety in Cu_2-DC-PyA we conducted relative viscosity experiments with stDNA (**Figure S20**). The Cu-free ligand, DC-PyA (**7**) showed a clear concentration-dependent increase in relative viscosity in line with the trend observed for established intercalators EtBr and actinomycin D. In contrast, the di-nuclear complex Cu_2-DC-PyA demonstrated a concentration-dependent decrease in relative viscosity, although this trend was less pronounced than that observed for the parent Cu_3-TC-Py. Data here support the additive bifunctional binding mode suggested by T_m studies. Overall, the observed decrease in viscosity associated with DNA condensation appears due to the electrostatic groove binding

properties of the di-copper(II) component overriding the lengthening properties associated with acridine intercalation.

View Article Online
DOI: 10.1039/D6CB00097E

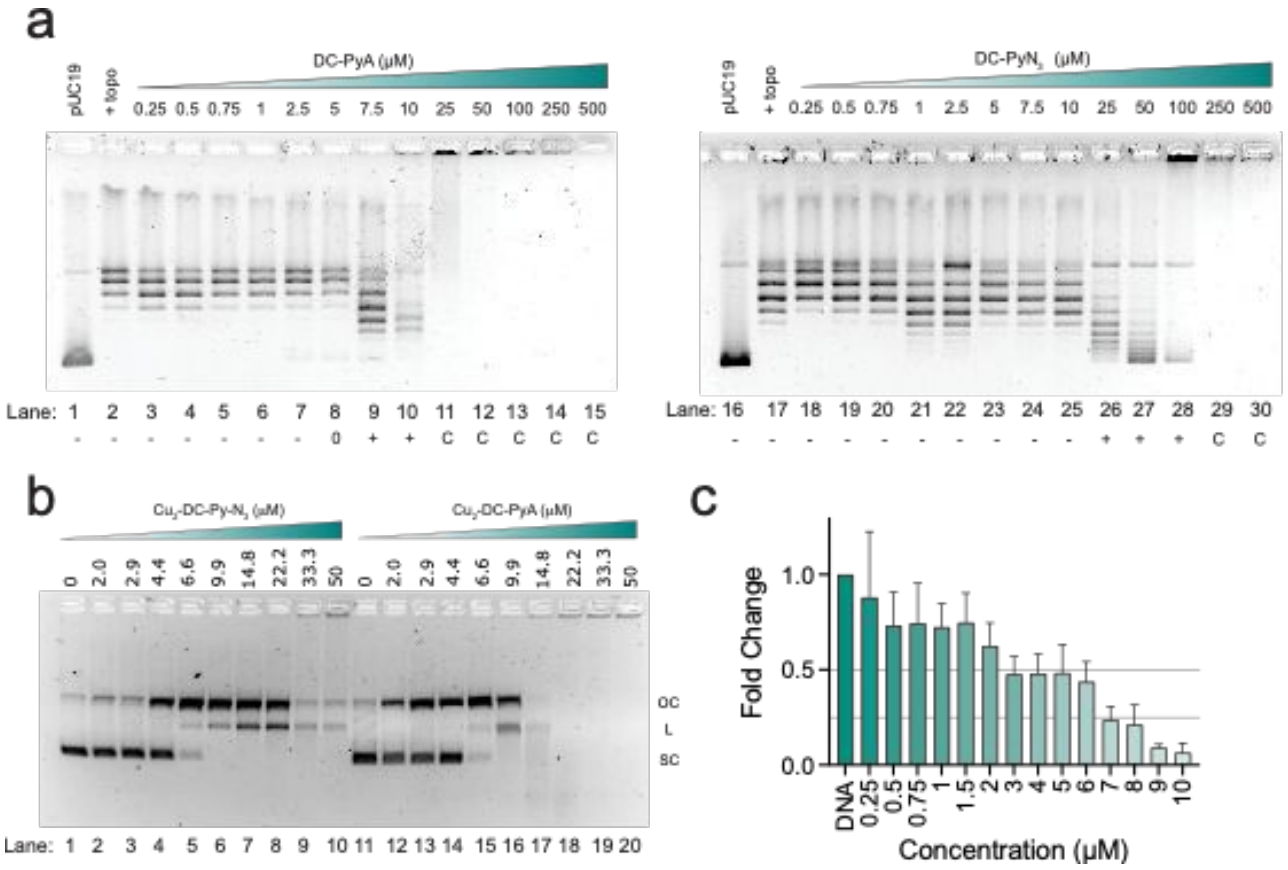

Figure 2: a) Release of topological tension from supercoiled plasmid DNA using the topoisomerase I-mediated relaxation assay in the presence of increasing concentrations of Cu_2-DC-PyA (left) and Cu_2-DC-PyN_3 (right). **b)** Supercoiled pUC19 cleavage profile of Cu_2-DC-PyN_3 (lanes 1-10) and Cu_2-DC-PyA (lanes 11-20). **c)** Relative quantification of cleavage induced by Cu_2-DC-PyA

Topoisomerase inhibition. To further investigate the intercalative properties of Cu_2-DC-PyA, a topoisomerase IA (Topo) mediated relaxation assay was performed.[36] Topo enzymes play an important role in regulating genome stability by relieving DNA topological constraints generated during processes such as gene transcription, DNA replication, recombination, and repair.[37] This is achieved through formation of a transient break in the DNA backbone, which permits topological relaxation, prior to strand ligation.[38] Unwinding of negatively supercoiled (SC) pUC19 DNA by Cu_2-DC-PyA was examined and compared to the non-acridine containing precursor, Cu_2-DC-PyN_3 (**Figure 2a**). Relaxation of the plasmid to the open circular form (0) was identified upon exposure to 5 μM of Cu_2-DC-PyA (lane 8). Higher concentrations of the complex (7.5 and 10 μM; lanes 9 and 10) generated positively (+) supercoiled DNA, beyond which the plasmid underwent condensation (lanes 11-15) presumably due to the high cationic charge borne by the hybrid. In contrast, Cu_2-DC-PyN_3 relaxed SC DNA between exposure values of 10 and 25 μM (lanes 10-11), indicating the acridine group plays an important role in enhancing the intercalating properties of the hybrid.

Artificial metallo-nuclease activity

pUC19 relaxation assay. The artificial metallo-nuclease activity of Cu_2-DC-PyA was initially evaluated using a electrophoretic mobility shift assay (EMSA).[39,40] Here, supercoiled pUC19 plasmid DNA was incubated with increasing concentrations of the complex, together with the exogenous reductant Na-*L*-ascorbate, and the conversion of supercoiled (SC) DNA to open-circular (OC) and linear (L) DNA forms was analysed by agarose gel electrophoresis. To understand how the acridine group impacts chemical nuclease activity, the DNA damage profile of Cu_2-DC-PyA was compared to Cu_2-DC-PyN_3 (**Figure 2b**). Experiments with Cu_2-DC-PyA showed formation of the nicked OC form at the lowest exposure (lane 12: 2.0 μM), while the L form, which arises due to the formation of double strand breaks, emerged at 6.6 μM (lane 15), with complete ablation observed at concentrations >9.9 μM (lanes 17-20). Next, the cleavage profile of Cu_2-DC-PyN_3 was monitored under identical conditions (lanes 2-10). Initially, the cleavage profile was similar to that of the acridine hybrid, with OC and L forms observed at 2.0 μM (lane 2) and 6.6 μM (lane 5), respectively. However, at concentrations >9.9 μM (lanes 7-10), larger fractions of OC and

L forms persist compared to Cu_2-DC-PyA treated samples. Overall, although both complexes are active chemical nucleases, it is clear the acridine hybrid outperforms the azide precursor, particularly at elevated concentrations.

Real-time PCR. Next, to quantify the DNA damage observed in the relaxation assay, the nuclease activity of Cu_2-DC-PyA was evaluated by real-time PCR (qPCR).[41–43] Here, a 411 bp amplicon from pUC19 was incubated with increasing concentrations (0.25-10 μM) of Cu_2-DC-PyA and Na-*L*-ascorbate at 37 °C for 30 min. Reactions were then quenched with EDTA and qPCR was performed and monitored in real time through SYBR Green I fluorescence. The threshold cycle (C_T) was determined, and the fold change in intact DNA was calculated and normalised to a non-treated control (**Figure 2c**). Significant damage was observed from 2 μM, with 50% of the amplicon depleted upon exposure to 3 μM and of the complex. Finally, just 25% of the amplicon remained at 7 μM with smaller fractions remaining thereafter. Overall, these data corroborate Cu_2-DC-PyA as an efficient artificial metallo-nuclease, capable of ablating DNA and preventing downstream processing by *Taq* DNA polymerase.

Groove blocking analysis. To probe the cleavage mechanism of Cu_2-DC-PyA, assays were performed in the presence of competitive DNA binding agents (**Figure 3a** and **S21**). Here, we employed methyl green and netropsin to probe the cleavage activity from the respective major and minor grooves,[44,45] while EtBr probed competition for intercalative sites and ActD acted as a dual competitor for intercalative sites and minor groove occupancy.[46–49] We observed that methyl green had no impact on cleavage activity while netropsin significantly inhibited cleavage by Cu_2-DC-PyA, suggesting that cleavage primarily occurs from the minor groove, similar to the parent Cu_3-TC-Py and earlier reported TC compounds. EtBr somewhat inhibited the activity while ActD was the most inhibitory competitor tested, with cleavage only observed at the highest tested concentration (20 μM). In total, these results further support the dual intercalative and minor groove binding modes suggested by thermal melting and viscosity studies and indicate Cu_2-DC-PyA retains the minor groove regiospecific cleavage activity found for other TC complexes.

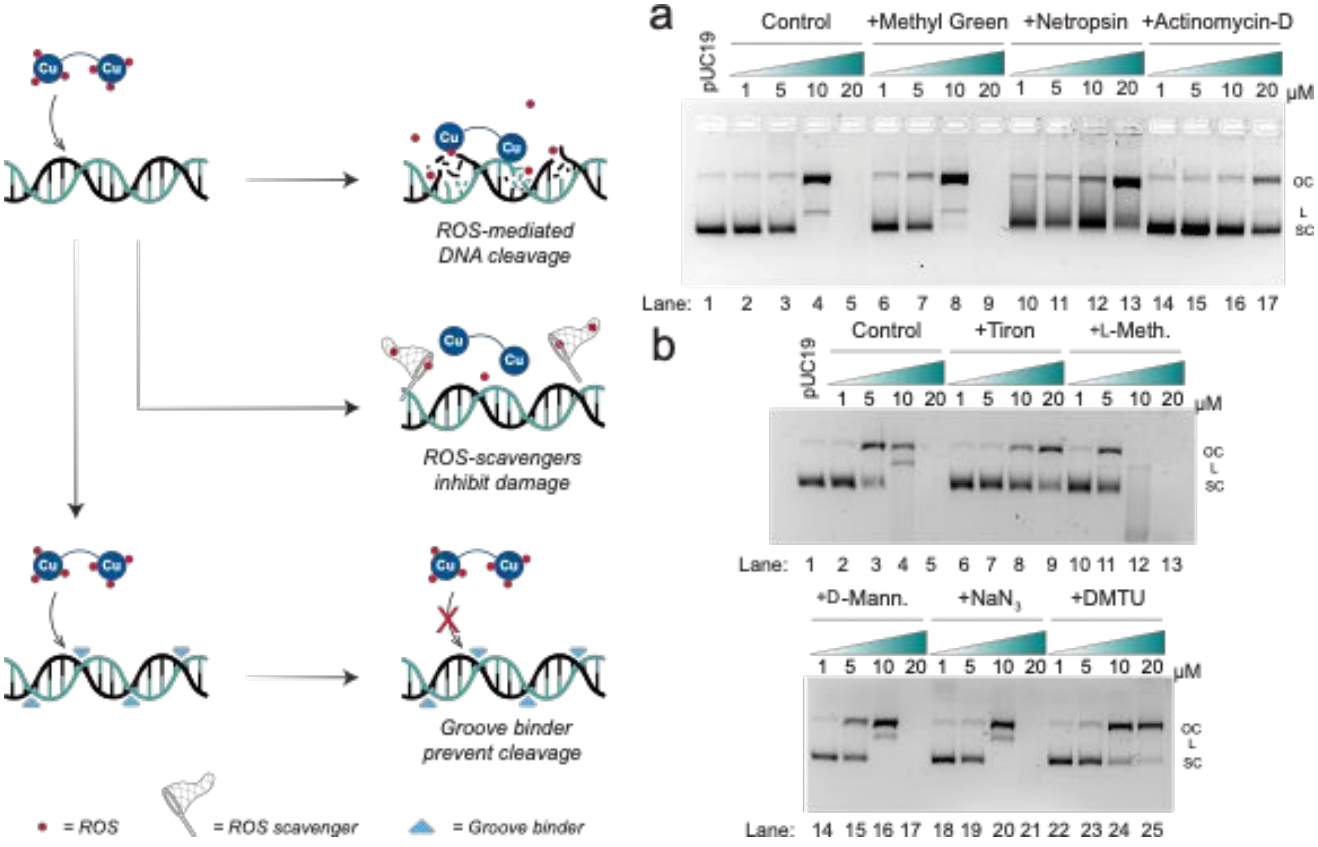

Figure 3: Cartoon representation of nuclease activity, and the impact of ROS scavengers and groove blocking groups. **a)** Agarose gel analysis of the Cu_2-DC-PyA (1, 5, 10 and 20 μM) cleavage of pUC19 (lanes 1-5) and Cu_2-DC-PyA (1, 5, 10 and 20 μM) cleavage of pUC19 DNA that was pre-treated with methyl green (lanes 6-9), netropsin (lanes 10-13) and actinomycin-D (lanes 14-17). **b)** Cleavage inflicted by Cu_2-DC-PyA (1, 5, 10 and 20 μM) on supercoiled plasmid DNA (lanes 1-5) that was pre-incubated with ROS scavengers tiron (lanes 6-9), L-methionine (lanes 10-13), D-mannitol (lanes 14-17), NaN_3 (lanes 18-21) and DMTU (lanes 22-25).

Scavenger studies. To determine the radical species involved in the Cu_2-DC-PyA cleavage pathway, experiments were performed using reactive oxygen species (ROS) scavengers:

Tiron (superoxide; $O_2^{\bullet-}$), L-methionine (hydroxyl radical; $^{\bullet}OH$, hypochlorous acid; HOCl, and hydrogen peroxide; H_2O_2); D-mannitol (hydroxyl radical; $^{\bullet}OH$); NaN_3 (singlet oxygen, $^1O_2$) and DMTU (hydrogen peroxide; H_2O_2 and the hydroxyl radical; $^{\bullet}OH$). Each ROS scavenger was added to pUC19 DNA prior to the addition of Cu_2-DC-PyA and Na-*L*-Ascorbate, and the cleavage profile was observed using the same EMSA protocol as in initial cleavage analysis (**Figure 3b**). A diminished cleavage profile was observed in the presence of tiron and DMTU, which implicates $O_2^{\bullet-}$, H_2O_2 and $^{\bullet}OH$ as the primary ROS involved in the cleavage pathway. Interestingly, we observed enhanced DNA damage in the presence of *L*-methionine. This activity might be linked to enhanced reduction of copper(II) by the thioether component of *L*-methionine, or that by sequestering both H_2O_2 and $^{\bullet}OH$, cleavage activity is activated through the more reactive $O_2^{\bullet-}$ pathway. This result is directly comparable to that of Cu_3-TC-Py, which demonstrates the mechanism is conserved upon the replacement of one Py unit with the acridine group.

Conclusions

Click chemistry has provided new avenues for the design and synthesis of metallodrugs, enabling the modular synthesis of artificial metallo-nucleases (AMNs) via a "click to chelate" strategy.[50,51] However, only a limited number of compounds have used the triazole group generated from the CuAAC reaction with proximal secondary donors to chelate Cu(II) ions. This concept was previously explored within our "Tri-Click" (TC) series, with recent work highlighting Cu_3-TC-Py as a leading AMN.[10–12] In the TC-Py study, molecular dynamics indicated that only two of the copper-chelating units in TC-Py could simultaneously bind with DNA, and in this work we exploited the opportunity to repurpose the third position with an acridine DNA intercalator. This resulted in the "Di-Click" (DC-PyA) derivative, a C_2-symmetric hybrid with augmented minor groove recognition and DNA intercalating properties. The primary aim of this work was to demonstrate that a significant change to the central modality of the TC series, reassembling one of the three arms to house a DNA-targeting intercalator with fluorescent properties could yield a new class of hybrid AMN. Ethidium bromide displacement assays revealed that Cu_2-DC-PyA displayed similar DNA binding affinity to the previous Cu_3-TC-Py and enhanced affinity compared to its azide-precursor (Cu_2-DC-PyN_3).

The binding profile of Cu_2-DC-PyA was further evaluated through FRET thermal melting where we observed a significant selectivity for GC-rich DNA. This enhanced selectivity for GC-rich DNA, relative to the parent Cu_3-TC-Py, indicated the acridine moiety was intercalating as intended and we further confirmed this in relative viscosity and topoisomerase I inhibition experiments. Viscosity experiments showed that the acridine group caused an increase in relative viscosity in the absence of Cu^{2+} ions and offset the decrease in the same relative to Cu_3-TC-Py. Topoisomerase studies further validated the addative effect of acridine conjugation with a markedly enhanced Topo I inhibition profile relative to the azide precursor. The DNA damaging properties of Cu_2-DC-PyA were assessed using a combination of qPCR and EMSA assays where again acridine conjugate showed significantly enhanced activity relative to the synthetic precursor. Mechanistic studies with ROS scavengers and competitive binders showed that Cu_2-DC-PyA retained the molecular mechanism and regioselectivity of Cu_3-TC-Py.

In the broader landscape of minor groove-directing hybrids, Cu_2-DC-PyA provides an interesting extension to established conjugates, such as Fe-EDTA-distamycin,[52] Cu-Phen-Hoechst-33258,[53] and the Cu-clip-phen-spermine series,[54] which utilise high-affinity binders to direct oxidative damage. However, the synthetic strategy reported here offers enhanced modularity and synthetic ease afforded by click chemistry. Furthermore, unlike traditional hybrids where the linker serves a purely structural role, the triazole moiety in DC-PyA is functionally integrated, serving both as a covalent bridge and as a donor group that chelates bioactive copper(II) ion; this approach simplifies the preparation of new hybrids and allows for the diversification of the DNA binding or directing unit. Consequently, this study may serve as a gateway to access more sophisticated systems. In summary, by repurposing the third chelating arm of Cu_3-TC-Py with a targeting unit, we have established a blueprint for generating future high-affinity, site-specific DNA damaging agents.

Experimental

General Remarks

All synthesis was conducted under atmospheric conditions unless otherwise stated. Chemical reagents were sourced from Merck, Tokyo Chemical Industry (TCI) and Fluorochem unless otherwise stated and were used without any further purification. Biological reagents were purchased from New England Biolabs or FisherScientific unless otherwise indicated. HPLC grade chloroform and methanol were used without further purification. ^1H and ^{13}C NMR spectra were obtained on a Bruker AC 600 MHz NMR spectrometer and processed in MNova (MastreLab). FTIR was performed on a PerkinElmer Spectrum Two FTIR. LC-MS was performed on an Agilent Technologies 1200 Series instrument consisting of a G1322A Quaternary pump and a G1314B UV detector (254 nm) coupled to an Advion Expression L Compact Mass spectrometer (ESI) operating in positive mode. Fluorescence quenching assays were performed on a TECAN Spark® microplate reader. Agarose gel electrophoresis was performed using a Bio-Rad wide-cell mini sub system with a Bio-Rad basic Power Pac™. All gels were imaged using a Syngene G:Box 9 mini gel documentation system. Real-time PCR (qPCR) and fluorescence thermal melting were performed on a Roche LightCycler 480 II.

Synthesis

*3,5-bis(bromomethyl)-2,4,6-trimethylphenol – **1** (**Dibromide**)*

To a solution of trioxane (0.661 g, 7.34 mmol), HBr (in acetic acid) (20 ml) was added slowly. The reaction was heated to 75 °C until fully dissolved. To the reaction, mesitylene (1 g, 7.34 mmol) and H_2O (0.833 ml) were added. The reaction was then refluxed at 125 °C for 3 h whilst stirring. The reaction was then allowed to cool to rt whilst

stirring. Ice cold water was then added to the reaction flask to form the precipitate. Vacuum filtration was used to remove excess water and dry the product resulting in a light brown powder. Yield: 92%. ^{1}H NMR (600 MHz, DMSO) δ 8.27 (s, 1H), 4.72 (s, 4H), 2.31 (s, 3H), 2.24 (s, 6H). **Figure S1**.

*3,5-bis(azidomethyl)-2,4,6-trimethylphenol – **2** (**Diazide**)*
To a solution of 3,5-bis(bromomethyl)-2,4,6-trimethylphenol (2.16 g, 6.72 mmol) in MeCN (30 ml), sodium azide (4.37 g, 67.17 mmol) was added slowly in the reaction flask. This reaction was then refluxed at 90 °C for 24 h whilst stirring. The resulting product was then filtered, and solvents removed by rotary evaporation leaving a brown solid. Yield: 94%. ^{1}H NMR (600 MHz, DMSO) δ 8.26 (s, 1H), 4.49 (s, 4H), 2.29 (s, 3H), 2.23 (s, 6H). FTIR: 2088 (s, N=N) cm^{-1}. **Figure S2**, **Figure S3**.

*2,4,6-trimethyl-3,5-bis((4-(pyridin-2-yl)-1H-1,2,3-triazol-1-yl)methyl)phenol - **3** (**DC-Py**)*
Diazide (1.53 g, 6.21 mmol) was dissolved in chloroform and methanol (1:1). Copper sulphate (0.050 g, 0.313 mmol) was dissolved in 1 mL of deionized water, and sodium ascorbate (0.100 g, 1.000 mmol) dissolved in 1 mL of deionized water. Copper sulphate solution was added dropwise to the sodium ascorbate solution (light blue – dark yellow/orange (reduction from copper(I) to copper(II))). Copper sulphate-sodium ascorbate solution was added dropwise to the diazide solution and stirred until dissolved. Ethynylpyridine (1.28 g, 12.43 mmol) was dissolved in chloroform and methanol (1:1) and subsequently added dropwise to the reaction flask. Round bottom flask flushed with nitrogen gas. Bung added to flask and left to stir at RT for 72 h. Product was then filtered and dried to give a beige solid. Yield: 71%. ^{1}H NMR (600 MHz, DMSO) δ 8.55 (s, 2H), 8.27 (s, 2H), 8.01 (s, 2H), 7.90 (s, 2H), 7.34 (s, 2H), 5.71 (s, 4H), 2.37 (s, 3H), 2.28 (s, 6H). **Figure S4**.

*2,2'-(((5-(4-bromobutoxy)-2,4,6-trimethyl-1,3 phenylene) bis(methylene))bis (1H-1,2,3-triazole-1,4-diyl))dipyridine – **4** (**DC-PyBr**)*
DC-Py (1.66 g, 3.67 mmol) was dissolved in acetonitrile (20 mL) (stirred with heat until dissolved), then sodium bicarbonate (3.08 g, 36.68 mmol) was added and dissolved. Subsequently, a solution of sodium hydroxide (0.09 g, 5.50 mmol) was added, followed by 1,4-dibromobutane (4.84 g, 22.01 mmol) in acetonitrile (20 mL). The reaction was then heated to 90 °C and refluxed and stirred overnight. The solution containing the product was then dried under rotary evaporation, dissolved in dichloromethane and washed with deionized water. It was then rinsed with portions of EDTA. The organic layer containing the product was then dried with magnesium sulphate. The resulting solution was then dried under rotary evaporation and then precipitated through dropwise addition to hexane solution and dried under vacuum. Yield: 28%. ^{1}H NMR (600 MHz, DMSO) δ 8.55 (ddd, *J* = 4.9, 1.8, 1.0 Hz, 2H), 8.34 (s, 2H), 8.00 (d, *J* = 7.9 Hz, 2H), 7.88 (td, *J* = 7.6, 1.8 Hz, 2H), 7.33 (ddd, *J* = 7.5, 4.8, 1.2 Hz, 2H), 5.73 (s, 4H), 3.71 (t, *J* = 6.4 Hz, 2H), 3.63 (t, *J* = 6.7 Hz, 2H), 2.39 (s, 3H), 2.35 (s, 6H), 2.07 – 2.00 (m, 2H), 1.92 – 1.84 (m, 2H). **Figure S5**.

*2,2'-(((5-(4-azidobutoxy)-2,4,6-trimethyl-1,3-phenylene)bis(methylene))bis(1H-1,2,3-triazole-1,4-diyl))dipyridine – **5** (**DC-PyN$_3$**)*
To a solution of DC-Py bromide (0.167 g, 0.285 mmol) in MeCN (20 ml), sodium azide (0.186 g, 2.85 mmol) was added slowly into the reaction flask. This reaction was then refluxed at 90 °C for 24 h whilst stirring. The resulting product was then filtered, and solvents were removed by rotary evaporation. Yield: 87%. ^{1}H NMR (600 MHz, CD_3CN) δ 8.51 (d, *J* = 4.0 Hz, 2H), 8.06 (d, *J* = 8.0 Hz, 4H), 7.83 (td, *J* = 7.8, 1.9 Hz, 2H), 7.29 – 7.27 (m, 2H), 5.69 (s, 4H), 3.73 (t, *J* = 6.3 Hz, 2H), 3.39 (t, *J* = 6.7 Hz, 2H), 2.39 (s, 3H), 2.35 (s, 6H), 1.89 – 1.77 (m, 4H). ^{13}C NMR (151 MHz, DMSO) δ 150.26, 150.00, 147.44, 137.69, 132.60, 131.56, 130.65, 123.49, 123.17, 119.92, 119.87, 51.04, 49.00, 27.37, 25.69, 16.08, 13.47, 13.16. FTIR: 2094 (s, N=N) cm^{-1}. **Figure S6**, **Figure S7**, **Figure S8**.

*N-(hex-5-yn-1-yl)acridin-9-amine – **6** (**Hexynyl acridine**)*
9-amine acridine (1.00 g, 5.15 mmol) and caesium carbonate (3.35 g, 10.30 mmol) were added to a round bottom flask with DMF and stirred until dissolved. 6-chlorohexyne (3.00 g, 25.74 mmol) was then added with triethylamine (50 mL) and ethanol. The reaction was left to stir at 70 °C for 96 hours. It was then filtered, and the solvent was removed in-vacuo. The crude product was purified by column chromatography to yield a yellow oil. Yield: 16.7%. ^{1}H NMR (600 MHz, $CDCl_3$) *δ*: 8.16 (d, 2H), 7.96 (d, 2H), 7.44 (d, 2H), 77.22 (t, 2H), 4.08 (t, 2H), 3.31 (d, 1H), 2.38 (t, 2H), 2.17 (t, 2H), 1.82 (t, 2H). **Figure S9**.

*N-(4-(1-(4-(2,4,6-trimethyl-3,5-bis((4-(pyridin-2-yl)-1H-1,2,3-triazol-1-yl)methyl) phenoxy) butyl)-1H-1,2,3-triazol-4-yl)butyl)acridin-9-amine – **7** (**DC-PyA**)*
DC-PyN$_3$ (0.258 g, 469 mmol) was dissolved in *tert*-butanol and water (1:1). Copper sulphate (0.852 g, 3.41 mmol) was dissolved in 1 mL of deionized water and sodium ascorbate (1.10 g, 0.555 mmol) was dissolved in 1 mL of deionized water. The copper sulphate solution was added dropwise to sodium ascorbate solution (light blue – dark yellow/orange (reduction from copper(II) to copper(I)). The copper sulphate-sodium ascorbate solution was added dropwise to the diazide solution and was stirred until dissolved. Hexyl acridine was dissolved in *tert*-butanol and water (1:1) and was added dropwise to the reaction flask. The reaction was stirred at room temperature for 4 h. The product was then filtered and dried. The crude product was purified by column chromatography, to give a yellow powder. Yield: 37.7%. ^{1}H NMR (600 MHz, $(CD_3)_2SO$) *δ*: 8.49 (d, 2H), 8.19 (m, 2H), 8.19 (m, 2H), 8.05 (d, 2H), 7.82 (d, 2H), 7.76 (m, 2H), 7.56 (s, 2H), 7.34 (s, 1H), 7.29 (t, 2H), 7.19 (t, 2H), 5.85 (s, 4H), 4.44 (t, 2H), 3.98 (t, 2H), 3.69 (t, 2H), 2.82 (t, 2H), 2.33 (s, 3H), 2.24 (s, 6H), 2.18 (m, 2H), 1.98 (m, 2H), 1.94 (m, 2H), 1.83 (m, 2H). ^{13}C NMR (151 MHz, $CDCl_3$) δ 153.73, 149.12, 148.13, 147.14, 146.31, 136.07, 132.83, 132.02, 131.97, 130.84, 129.39, 123.02, 121.99, 121.94, 120.21, 120.13, 120.09, 120.02, 119.32, 71.02, 49.00, 48.48, 48.03, 29.03, 26.25, 26.20, 26.14, 25.27, 23.86, 14.80, 11.99. ESI-MS: $[M+H]^+$ m/z calculated = 824.5, found = 824.5. **Figure S10**, **Figure S11**, **Figure S12**.

Fluorescence Competition assay

EtBr displacement assays were carried out using methods previously reported. In 96 well plates, a serial dilution of each complex was prepared to a volume of 50 μL in 80 mM HEPES, 25 mM NaCl with 5% DMSO. To this, 50 μL of a working solution containing 25 μM EtBr and 25 μM ctDNA in the same buffer was added to give final conditions of 12.5 μM EtBr, 12.5 μM CT-DNA and varying analyte concentration in a volume of 100 μL. Blank wells were prepared to contain no DNA and control wells contained no titrant / analyte. Plates were allowed to equilibrate for 30 min prior to fluorescence measurements using excitation at 530 nm and detection 590 nm. Resulting data was modelled using non-linear regression in GraphPad Prism and used to calculate K_{app} values as reported. Data plotted of TC-Py was obtained from the source data of previously reported K_{app} values of TC-Py[7] to allow for direct comparison of apparent binding.

Direct DNA binding analysis

The binding affinity of Cu_2-DC-PyA was analysed by monitoring fluorescence upon titration of ctDNA. In 96-well plate, samples were prepared to contain varying concentrations of ctDNA via serial dilution. 50 μL of a 20 μM Cu_2-DC-PyA solution was then added. Plates were incubated at RT for 30 min before reading fluorescence intensity (excitation / emission: 415 / 455 nm). Final conditions: 100 μL volume, varying ctDNA concentration, 10 μM Cu_2-DC-PyA, 80 mM HEPES, 25 mM NaCl, pH 7.4. Data was normalised to provide a plot of fraction bound versus ctDNA concentration and the resulting data was fit in GraphPad prism using equations 2 and 3. **Figure S13-16**.

$$\textbf{Equation 2)}\ Y = \frac{(b - \sqrt{b^2 - 2K^2Dn^{-1}})}{2KD}$$

$$\textbf{Equation 3)}\ b = 1 + KD + \frac{KX}{2n}$$

Where Y is the fraction bound, K is the binding affinity, D the concentration of the target DNA (Cu_2-DC-PyA), N is the binding site size or stoichiometry and X is the concentration of titrant (ctDNA).

Fluorescence Resonance Energy Transfer (FRET) Melting

Thermal melting analysis was performed on a Roche LightCycler®480 II using 80 mM HEPES 25 mM NaCl buffer. Prior to analysis DNA hairpins were denatured by heating to 90 °C (10 °C/min, 2 min hold) and reannealed at 12 °C (0.5 °C/min, 20 min hold). A serial dilution of Cu_2-DC-PyA (highest concentration = 10 μM) was performed and FRET-labelled hairpin was added to a final concentration 1 μM. Melting was conducted in triplicate at a ramp rate of 0.5 °C min^{-1} up to a maximum of 95 °C. T_m values were calculated from the midpoint of the melting curves, which was found at the peak of the first derivative.

DDH – 5'-F-CGCGAATTCGCGAAAAACGCGAATTCGCG-Q-3'

D6aH - 5'-F-GCATTATAATGCAAAAAGCATTATAATGC-Q-3'

A schematic of the FRET melting analysis of the FRET hairpins can be seen in **Figure S18**, where F = Alexa fluor 647 and Q = Iowa black quencher.

Topoisomerase IA relaxation

Topoisomerase IA (topo) relaxation was performed as previously reported with slight modification[22]. In a total volume of 15 μL, pUC19 supercoiled plasmid DNA (400 ng) and increasing concentrations (0.25-500 μM) of drug (Cu_2-DC-Py-HA, Cu_2-DC-Py-N_3 or Cu_2-DC-Py-Br + HA) were incubated in HEPES buffer (80 mM, pH 7.2) at 37 °C for 30 min. rCutsmart (1×, NEB) and topo IA (1 U, NEB) were added and samples were incubated at 37 °C for 20 min. The topo enzyme was heat inactivated at 65 °C for 30 min. DNA loading buffer (6×, 10 mM Tris-HCl, pH 7.6, 0.03%bromophenol blue, 0.03% xylene cyanol FF, 60% glycerol, 60 mM EDTA) was added and samples were loaded onto a 1.2% agarose gel (1× TBE) and run at 40 V for 3 h, followed by 50 V for 2.5 h. The gel was post-stained in SYBRsafe™ (1×) for 20 min, followed by de-staining in deionised (DI) H_2O for 20 min. Images were captured on a UV transilluminator.

Viscosity studies

To determine how various compounds effect the viscosity of DNA, a DV-II-Programmable Digital Viscometer equipped with Enhanced Brookfield UL Adapter was used. This method was carried out at 60 rpm using spindle #0 in working samples of 15 mL stDNA (deoxyribonucleic acid sodium salt from salmon testes, Sigma-Aldrich, D1626) prepared at 1 mM in 80 mM HEPES buffer. Stock solutions of each compound were titrated into the stDNA at increasing [drug]/[DNA] (*r*) ratios of 0.02, 0.04, 0.06, 0.08, 0.1, 0.12, 0.14, 0.16, 0.18, and 0.2. Titrations were carried out directly into the viscometer with constant stirring and left for 10 min before readings were taken, thus allowing for drug-DNA binding equilibrium to be reached. Data were then plotted using η/η_o against [drug]/[DNA] ratios, in which η refers to the cP value in the presence of drug, and η_o refers to the initial cP value without titrant.

DNA Cleavage

In a total volume of 20 μL (80 mM HEPES, 25 mM NaCl) Cu_2-DC-Py-HA or Cu_2-DC-Py-azide (2.6-100 μM), pUC19 plasmid DNA (400 ng) and Na-*L*-Ascorbate (1 mM) were incubated 37 °C for 30 minutes. Loading dye (6×, 10 mM Tris-HCl, 0.03% bromophenol blue, 0.03% xylene cyanole FF, 60% glycerol, 60 mM EDTA) was added and samples were loaded onto a 1.3% agarose gel (1× TAE) containing SYBRsafe™. Gel was run at 70 V for 90 min prior to visualisation on a UV transilluminator.

Groove Blocking

Samples were prepared as described above at Cu_2-DC-Py-HA (1, 5, 10, 20 μM), but methyl green (8 μM), netropsin (8 μM), actinomycin-D (8 μM) or EtBr (8 μM) were added prior to addition of Cu_2-DC-Py-HA. Samples were incubated at 37 °C for 30 min and analysed by

agarose gel electrophoresis (1.3% agarose, 1× TAE, 70 V for 90 min). Loading dye (6×, 10 mM Tris-HCl, 0.03% bromophenol blue, 0.03% xylene cyanole FF, 60% glycerol, 60 mM EDTA) was added and gel was visualised.

Reactive oxygen species (ROS) scavengers

Samples were prepared as described above at Cu_2-DC-PyA (1, 5, 10, 20 μM), but ROS scavengers (1 mM) were added prior to addition of Cu_2-DC-Py-HA. Samples were incubated at 37 °C for 30 min. and analysed by agarose gel electrophoresis (1.3% agarose, 1× TAE, 70 V for 90 min). Loading dye (6×, 10 mM Tris-HCl, 0.03% bromophenol blue, 0.03% xylene cyanole FF, 60% glycerol, 60 mM EDTA) was added and gel was visualised.

Real-time quantitative PCR (qPCR)

A 411bp amplicon of pUC19 (forward: 5′-TGACTCCCCGTCGTGTAGAT-3′ and reverse: 5′-TGATAACACTGCGGCCAACT-3′) was generated by PCR (PCR Biosystems) and purified using membrane spin columns (Monarch PCR & DNA clean-up kit, NEB). The 411 bp amplicon (200 ng) was diluted to 8 μL in HEPES (80 mM, pH 7.2). Half of the sample volume (4 μL) was removed and kept as reference samples. The remaining 4 μL incubated with increasing concentrations of Cu_2-DC-Py-HA (0.25-10 μM) and Na-*L*-ascorbate (1 mM). Samples were incubated at 37 °C for 30 min and quenched with EDTA (1 mM). Diluted ($1{:}4^3$) reference and experimental samples were analysed by qPCR through amplification of a 254 bp region (forward: 5′-CAGTGCTGCAATGATACCGC-3′ and reverse: 5′-GGGAACCGGAGCTGAATGAA-3′) over 45 cycles through SYBR green I fluorescence (SYBR green I master, Roche). The changes in C_T (threshold cycle) between experiment and reference samples (experiment C_T–reference C_T) were calculated (ΔC_T). ΔC_T was then normalised to a non-treated control (ΔC_Tsample - ΔC_Tcontrol = $\Delta\Delta C_T$), and this was plotted as a linear value $2^{-\Delta\Delta CT}$. Ordinary one-way ANOVA with Dunnett's multiple comparisons was performed, using GraphPad Prism, to determine the significance of the $2-\Delta\Delta C$values obtained. * = P = < 0.05, significant ** = P < 0.01, very significant. *** = P < 0.001, extremely significant.

Author contributions

OG: Formal analysis, writing (original content, reviewing and editing), AG: Funding acquisition, formal analysis, writing (original content, review and editing), conceptualisation, supervision, project administration, methodology. RL: Formal analysis. SP: Formal analysis, supervision, conceptualisation, writing (review and editing). BMcG: Funding acquisition, formal analysis, writing (original content, review and editing), methodology, supervision, project administration. AK: Funding acquisition, writing (review and editing), supervision, project administration, conceptualisation.

Conflicts of interest

There are no conflicts to declare.

View Article Online
DOI: 10.1039/D6CB00097E

Data availability

All data related to this article is included in the article or supplementary files. Raw data files are available on request from the corresponding authors.

Acknowledgements

AG acknowledges funding from the Research Ireland postdoctoral fellowship programme (GOIPD/2025/1020). BMcG and AK acknowledge funding from Research Ireland ARC-HUB for Therapeutics (23/ARC/11991). AK acknowledges funding from the MSCA-DN (HE2021-27) MeChaNiSM (101168851) and the Novo Nordisk Foundation (NNF19OC0056845).

References

1 A. Gibney and A. Kellett, *Chem. Eur. J.*, 2024, **30**, e202401621.
2 S. Poole, O. A. Aning, V. McKee, T. Catley, A. Y. Nielsen, H. Thisgaard, P. Johansson, G. Menounou, J. Hennessy, C. Slator, A. Gibney, A. Pyne, B. McGorman, F. Westerlund and A. Kellett, *Nucleic Acids Res.*, 2025, **53**, gkae1250.
3 R. Lynn, A. Gibney, E. Delahunt, S. MacDonald-Brown, C. Lence, M. Kenny, M. Allen, R. Khaybullin, I. Lukac, A. Jordan and A. Kellett, *Chembiochem*, 2026, **27**, e202500874.
4 J.-T. Wang, Q. Xia, X.-H. Zheng, H.-Y. Chen, H. Chao, Z.-W. Mao and L.-N. Ji, *Dalton Trans.*, 2010, **39**, 2128–2136.
5 C. B. Chen, L. Milne, R. Landgraf, D. M. Perrin and D. S. Sigman, *Chembiochem*, 2001, **2**, 735–740.
6 F. Mancin, P. Scrimin, P. Tecilla and U. Tonellato, *Chem. Commun. (Camb.)*, 2005, 2540–2548.
7 J. Chen and J. Stubbe, *Nat. Rev. Cancer*, 2005, **5**, 102–112.
8 S. M. Hecht, *J. Nat. Prod.*, 2000, **63**, 158–168.
9 H. Umezawa, K. Maeda, T. Takeuchi and Y. Okami, *J. Antibiot. (Tokyo)*, 1966, **19**, 200–209.
10 N. McStay, C. Slator, V. Singh, A. Gibney, F. Westerlund and A. Kellett, *Nucleic Acids Res.*, 2021, **49**, 10289–10308.
11 A. Gibney, R. E. F. de Paiva, V. Singh and R. Fox, *Angew. Chem. Int. Ed Engl.*
12 A. Gibney, M. Sidarta, E. Delahunt, P. Mesdom, L. Arrué, S. Kk, O. A. Aning, H. Hjerpe, F. Figueiredo, K. Cariou, V. McKee, P. Johansson, S. Bhattacharya, D. Thompson, M. Wenzel, G. Gasser, F. Westerlund and A. Kellett, *Nat. Commun.*, 2026, **17**, 2309.
13 J. Hennessy, P. Klimkowski, D. Singleton, A. Gibney, M. Coche, N. P. Farrell, A. H. El-Sagheer, T. Brown and A. Kellett, *RSC Med. Chem.*, 2024, **15**, 485–491.
14 N. Zuin Fantoni, B. McGorman, Z. Molphy, D. Singleton, S. Walsh, A. H. El-Sagheer, V. McKee, T. Brown and A. Kellett, *Chembiochem*, 2020, **21**, 3563–3574.
15 B. McGorman, N. Z. Fantoni, S. O'Carroll, A. Ziemele, A. H. El-Sagheer, T. Brown and A. Kellett, *Nucleic Acids Res.*, 2022, **50**, 5467–5481.
16 M. Huynh, R. Vinck, B. Gibert and G. Gasser, *Adv. Mater.*, 2024, e2311437.
17 G. Roelfes, M. E. Branum, L. Wang, L. Que and B. L. Feringa, *J. Am. Chem. Soc.*, 2000, **122**, 11517–11518.

18 S. A. Ross, M. Pitié and B. Meunier, *Eur. J. Inorg. Chem.*, 1999, **1999**, 557–563.
19 C. Boldron, S. A. Ross, M. Pitié and B. Meunier, *Bioconjug. Chem.*, 2002, **13**, 1013–1020.
20 Y. Huang, Y. Zhang, J. Zhang, D.-W. Zhang, Q.-S. Lu, J.-L. Liu, S.-Y. Chen, H.-H. Lin and X.-Q. Yu, *Org. Biomol. Chem.*, 2009, **7**, 2278–2285.
21 Q. Liu, J. Zhang, M.-Q. Wang, D.-W. Zhang, Q.-S. Lu, Y. Huang, H.-H. Lin and X.-Q. Yu, *Eur. J. Med. Chem.*, 2010, **45**, 5302–5308.
22 S. A. Pérez, C. de Haro, C. Vicente, A. Donaire, A. Zamora, J. Zajac, H. Kostrhunova, V. Brabec, D. Bautista and J. Ruiz, *ACS Chem. Biol.*, 2017, **12**, 1524–1537.
23 L. Do Quental, E. Palma, M. C. Oliveira and F. Mendes, *Sci. Rep.*
24 K. Walsh, H. F. Sneddon and C. J. Moody, *ChemSusChem*, 2013, **6**, 1455–1460.
25 Y. Cheng and W. H. Prusoff, *Biochem. Pharmacol.*, 1973, **22**, 3099–3108.
26 A. Kellett, Z. Molphy, C. Slator, V. McKee and N. P. Farrell, *Chem. Soc. Rev.*, 2019, **48**, 971–988.
27 M. T. Carter, M. Rodriguez and A. J. Bard, *J. Am. Chem. Soc.*, 1989, **111**, 8901–8911.
28 M. T. Carter and A. J. Bard, *J. Am. Chem. Soc.*, 1987, **109**, 7528–7530.
29 R. A. J. Darby, M. Sollogoub, C. McKeen, L. Brown, A. Risitano, N. Brown, C. Barton, T. Brown and K. R. Fox, *Nucleic Acids Res.*, 2002, **30**, e39.
30 T. D. Prieto Otoya, K. T. McQuaid, J. Hennessy, G. Menounou, A. Gibney, N. G. Paterson, D. J. Cardin, A. Kellett and C. J. Cardin, *Angew. Chem. Int. Ed Engl.*, 2024, **63**, e202318863.
31 A. Guédin, L. Lacroix and J.-L. Mergny, *Methods Mol. Biol.*, 2010, **613**, 25–35.
32 W. D. Wilson, F. A. Tanious, M. Fernandez-Saiz and C. T. Rigl, *Methods Mol. Biol.*, 1997, **90**, 219–240.
33 C. Bailly, W. A. Denny, L. E. Mellor, L. P. Wakelin and M. J. Waring, *Biochemistry*, 1992, **31**, 3514–3524.
34 L. S. Lerman, *J. Mol. Biol.*, 1961, **3**, 18–30.
35 D. Suh and J. B. Chaires, *Bioorg. Med. Chem.*, 1995, **3**, 723–728.
36 P. Peixoto, C. Bailly and M.-H. David-Cordonnier, *Methods Mol. Biol.*, 2010, **613**, 235–256.
37 B. K. Sinha, *Drugs*, 1995, **49**, 11–19.
38 L. Stewart, M. R. Redinbo, X. Qiu, W. G. Hol and J. J. Champoux, *Science*, 1998, **279**, 1534–1541.
39 H. Kuhn, E. Protozanova and V. V. Demidov, *Electrophoresis*, 2002, **23**, 2384–2387.
40 L. M. Hellman and M. G. Fried, *Nat. Protoc.*, 2007, **2**, 1849–1861.
41 W. Wang, K. Scheffler, Y. Esbensen and L. Eide, *Methods Mol. Biol.*, 2016, **1351**, 27–32.
42 S. O. Evans, M. B. Jameson, R. T. M. Cursons and L. M. Peters, *Biology (Basel)*.
43 A. G. Mutlu, *Polymerase Chain Reaction. InTech, Rijeka*.
44 S. K. Kim and B. Nordén, *FEBS Lett.*, 1993, **315**, 61–64.
45 C. M. Nunn, E. Garman and S. Neidle, *Biochemistry*, 1997, **36**, 4792–4799.
46 J. Olmsted 3rd and D. R. Kearns, *Biochemistry*, 1977, **16**, 3647–3654.
47 M. Gellert, C. E. Smith, D. Neville and G. Felsenfeld, *J. Mol. Biol.*, 1965, **11**, 445–457.
48 T. R. Krugh, *Proc. Natl. Acad. Sci. U. S. A.*, 1972, **69**, 1911–1914.
49 S. Kamitori and F. Takusagawa, *J. Mol. Biol.*, 1992, **225**, 445–456.
50 C. A. Kluba and T. L. Mindt, *Molecules*, 2013, **18**, 3206–3226.
51 T. L. Mindt, H. Struthers, L. Brans, T. Anguelov, C. Schweinsberg, V. Maes, D. Tourwé and R. Schibli, *J. Am. Chem. Soc.*, 2006, **128**, 15096–15097.
52 P. G. Shultz, J. S. Taylor and P. B. Dervan, *J. Am. Chem. Soc.*, 1982, **104**, 6861–6863.
53 C. H. Chen, A. Mazumder, J. F. Constant and D. S. Sigman, *Bioconjug. Chem.*, 1993, **4**, 69–77.
54 M. Pitié and B. Meunier, *Bioconjug. Chem.*, 1998, **9**, 604–611.

View Article Online
DOI: 10.1039/D6CB00097E

Data availability statement for:

Rational Design of an Acridine-derived Click Chemistry-based Artificial Metallo-Nuclease

All data supporting the findings of this study are available within the article and its Electronic Supplementary Information (ESI). The ESI includes full experimental procedures, NMR spectra, FT-IR spectra, LC-MS data, fluorescence binding data, FRET melting curves, and gel electrophoresis images supporting the synthesis, characterisation, and biological assays described in the manuscript. Additional raw datasets generated or analysed during the current study are available from the corresponding authors upon reasonable request.